Chaos and the quantum-classical correspondence in the kicked pendulum

Ronald F. Fox and T. C. Elston
School of Physics, Georgia Institute of Technology, Atlanta, Georgia 30332-0430
(Received 2 February 1994)

The problem of determining the quantum signature of a classically chaotic system is studied for the periodically kicked pendulum. In parallel with the observation that chaos creates exponential growth of intrinsic fluctuations in classical, macroscopic, dissipative systems, we find that the quantum variances initially grow exponentially if the corresponding classical description is chaotic. The rate of growth is connected to the corresponding classical Jacobi matrix and, thereby, to the largest classical Liapunov exponent. These connections are established by examining the correspondence between the quantum Husimi-O'Connell-Wigner distribution and the classical Liouville distribution for an ensemble. Explicit results for the kicked pendulum are presented.

PACS number(s): 05.45.+b, 03.65.Bz

I. INTRODUCTION

In a series of recent papers [1–3], it has been demonstrated that the covariances of the intrinsic fluctuations in classical, macroscopic, dissipative systems initially grow exponentially when the system is chaotic. The connection between chaos and the growth of fluctuations depends upon the central role played by the Jacobi matrix [3] in both the theories for chaos and for fluctuations. This quantity is simultaneously responsible for determining: (a) whether or not the largest Liapunov exponent is positive (we take this characteristic to be the definition of chaos for systems with bounded phase-space flows), and (b) the rate of time evolution of the fluctuation covariances. To establish this connection, it is necessary to extract the classical, macroscopic description from an underlying mesoscopic description given by a master equation [4]. As a result, it is seen how the macroscopic equations *emerge* from the mesoscopic description in an appropriate limit. In addition, other limits [5,6] provide the dynamics for the associated intrinsic fluctuations.

It has already been observed [3] that the quantum-classical correspondence for a potentially chaotic, conservative, classical system can be expressed in terms of the correspondence [7] between the time evolution of the Wigner distribution and the Liouville equation for the time evolution of a classical phase-space distribution. It was shown [3] that the initial rate of growth of quantum variances was directly tied to the time evolving Jacobi matrix for the classical motion. In this paper, we refine this connection by focusing on the Husimi-O'Connell-Wigner [8,9] distribution and its more precise correspondence with Liouville's equation for an initially Gaussian ensemble. The Gaussian ensemble reflects the unavoidable uncertainty in initial conditions. This uncertainty is intrinsic to both the quantum and the classical descriptions. We also show that statistics obtained from the time evolution of the Husimi-O'Connell-Wigner distribution can be realized numerically much more efficiently by following the time evolution of an appropriately constructed, initially Gaussian, wave packet. This circumstance parallels the relative ease with which it is possible to numerically implement the Fokker-Planck equation and its associated Langevin equivalent.

In this paper, these general and rather formal considerations are exhibited by the periodically kicked pendulum [10]. It is important to emphasize that our exponential growth results are not in conflict with the well-known diffusive growth rates so often quoted in the literature [11,12] for the chaotic parameter domain of the kicked pendulum. This difference is a result of effectively different initial conditions and we show that for initially sharp Gaussian distributions, there is always an initial exponential growth stage, possibly followed by a transition into a diffusive stage. This is dramatically exhibited in our numerical results where we show, for the ultrasupercritical parameter regime, the exponential growth of the variances around a subcritically stable elliptical center. We also obtain a quantitative connection between the rate of growth of the quantum variances during the exponential stage and the transient expansion rate [13–15].

With these results, we establish the efficacy in characterizing "the quantum signature of classical chaos" by the initially exponential growth of quantum variances for initially sharp wave packets.

II. THE CENTRAL ROLE OF THE JACOBI MATRIX

A. Classical chaos

In this section, the central role played by the Jacobi matrix is reviewed. Consider a macroscopic description given in terms of N coupled nonlinear ordinary differential equations

$$\frac{d}{dt}x_i(t)=F_i(\mathbf{x}(t)) \tag{1}$$

in which the index i has N possible values and the forcing functions, F_i, are generally nonlinear. Even partial differential equations can be rendered in this form, at least approximately (e.g., by mode expansions followed by Galerkin truncations). If the flow described by Eq. (1)

is bounded, then we take as the definition of chaos the existence of a positive largest Liapunov exponent, λ. This means that very small initial differences, $\Delta\mathbf{x}(0)$, in initial conditions grow exponentially, at least until the threshold for nonlinearities is crossed:

$$\Delta\mathbf{x}(t)\sim e^{\lambda t}\Delta\mathbf{x}(0) \ . \tag{2}$$

Underlying this exponential growth is the Jacobi matrix for the flow, J_{ik}, defined by

$$J_{ik}(\mathbf{x}(t))=\frac{\partial F_i(\mathbf{x}(t))}{\partial x_k(t)} \ . \tag{3}$$

It is easy to show that $\Delta\mathbf{x}(t)$ satisfies the equation

$$\frac{d}{dt}\Delta x_i=J_{ik}(\mathbf{x}(t))\Delta x_k \ , \tag{4}$$

which has the solution

$$\Delta\mathbf{x}(t)=\exp_T\left[\int_0^t ds\mathbf{J}(\mathbf{x}(s))\right]\Delta\mathbf{x}(0) \ , \tag{5}$$

in which $\exp_T(\ )$ denotes the forward-in-time time ordered exponential. Together, Eqs. (2) and (5) demonstrate the fundamental dependence of the largest Liapunov exponent on the time evolving Jacobi matrix. We return to this issue in Sec. IV D.

B. The Kramers-Moyal expansion for the master equation

Any macroscopic description such as given by Eq. (1) describes deterministic dynamics without any account being made for possible fluctuations. Since the underlying microscopic dynamics is both molecular and thermal, there are necessarily intrinsic fluctuations associated with the deterministic dynamics. One very general way to formalize this physical circumstance is to extract Eq. (1) from an underlying mesoscopic dynamics given by a master equation [4]. This equation describes the time evolution of a probability distribution, $P(\mathbf{x},t)$, for the fluctuating values of $\mathbf{x}(t)$.

$$\frac{\partial}{\partial t}P(\mathbf{x},t)=\int d^N x'[W(\mathbf{x},\mathbf{x}')P(\mathbf{x}',t)-W(\mathbf{x}',\mathbf{x})P(\mathbf{x},t)] \ , \tag{6}$$

in which $W(\mathbf{x},\mathbf{x}')$ denotes the transition rates from $\mathbf{x}'$ values to $\mathbf{x}$ values. For processes called jump processes, $W(\mathbf{x},\mathbf{x}')$ is nonzero only for molecular sized transitions. This property can be formalized by introducing the W moments, $K^{(n)}_{i_1 i_2\cdots i_n}$, defined by

$$\begin{aligned}K^{(n)}_{i_1 i_2\cdots i_n}&=\int d^N x'(x'_{i_1}-x_{i_1})\\&\quad\times(x'_{i_2}-x_{i_2})\cdots(x'_{i_n}-x_{i_n})W(\mathbf{x},\mathbf{x}')\\&\sim\Omega^{-(n-1)} \ ,\end{aligned} \tag{7}$$

in which Ω denotes the system size and in which the fall off of the higher moments with system size is indicated. This leads to the Kramers-Moyal expansion [4] for the master equation as an infinite order partial differential equation

$$\frac{\partial}{\partial t}P(\mathbf{x},t)=\sum_{n=1}^{\infty}\frac{(-1)^n}{n!}\prod_{j=1}^{n}\frac{\partial}{\partial x_{k_j}}(K^{(n)}_{k_1 k_2\cdots k_n}(\mathbf{x})P(\mathbf{x},t)) \ . \tag{8}$$

C. The macroscopic limit of the Kramers-Moyal expansion

The Ω scaling of the W moments given in Eq. (7) leads to the $\Omega\to\infty$ macroscopic limit approximation for the master equation given by

$$\frac{\partial}{\partial t}P(\mathbf{x},t)=-\frac{\partial}{\partial x_k}[K^{(1)}_k(\mathbf{x})P(\mathbf{x},t)] \ . \tag{9}$$

This partial differential equation has the very special property that it is first order in both the t derivative and in the x_k derivatives. This means that it can have Dirac δ function solutions

$$P(\mathbf{x},t)=\delta(\mathbf{x}-\mathbf{x}(t)) \ , \tag{10}$$

in which $x_i(t)$ satisfies the equation

$$\frac{d}{dt}x_i(t)=K^{(1)}_i(\mathbf{x}(t)) \ . \tag{11}$$

Thus, we can say that the macroscopic description, Eq. (1), has *emerged* from the underlying master equation if we identify the macroscopic forcing functions, F_i, with the first W moment, $K^{(1)}_i$, i.e.,

$$F_i=K^{(1)}_i \ . \tag{12}$$

D. Central limit theorem treatment of the fluctuations

Obviously the macroscopic limit is too severe since it completely eliminates the fluctuations. A central limit theorem exists for the fluctuations [4]. This limit is also called the van Kampen system size expansion and is an expansion in the smallness parameter $\Omega^{-1/2}$. The time evolution for the probability distribution, $\Phi(\mathbf{y},t)$, for the scaled deviations, $\mathbf{y}$, from the deterministic solutions, $\mathbf{x}(t)$, is given by the linear Fokker-Planck equation (by linear, we mean a linear streaming term, the $K^{(1)}_i$ term)

$$\begin{aligned}\frac{\partial}{\partial t}\Phi(\mathbf{y},t)=&-\frac{\partial}{\partial y_i}\left[\frac{\partial}{\partial x_j}K^{(1)}_i(\mathbf{x}(t))y_j\Phi(\mathbf{y},t)\right]\\&+\frac{1}{2}\frac{\partial^2}{\partial y_i\partial y_j}[R^{(2)}_{ij}(\mathbf{x}(t))\Phi(\mathbf{y},t)] \ ,\end{aligned} \tag{13}$$

where

$$\mathbf{x}=\mathbf{x}(t)+\Omega^{-1/2}\mathbf{y} \tag{14}$$

and

$$R^{(2)}_{ij}(\mathbf{x}(t))=\lim_{\Omega\to\infty}\Omega K^{(2)}_{ij}(\mathbf{x}(t)) \ . \tag{15}$$

This limit theorem provides the dynamics of the fluctuations in the small fluctuation regime. This is reflected by the fact that the streaming term of the equation is linear in the y_j's. Moreover, both the first and second W moment factors are evaluated as functions of the deterministic solutions $\mathbf{x}(t)$. Note, in particular, [cf. Eq. (12)] that

the y_j coefficients in the first term on the right-hand side are precisely the Jacobi matrix elements for the deterministic flow.

E. The time evolution of the covariance matrix

The covariance matrix for the fluctuations at time t is defined by

$$C_{ij}(t)=\langle y_i y_j \rangle_t \ , \tag{16}$$

in which $\langle \ \rangle_t$ denotes averaging with respect to the distribution $\Phi(\mathbf{y},t)$. The time evolution of C_{ij} follows directly from the Eq. (13):

$$\frac{d}{dt}C_{ik}(t)=J_{ij}(t)C_{jk}(t)+C_{ij}(t)J_{kj}(t)+R_{ik}^{(2)}(t) \ . \tag{17}$$

We have previously shown [3] that chaos in the deterministic flow implies exponential initial growth of the covariances at a rate that is twice the largest positive Liapunov exponent for the deterministic flow. This is directly a result of the presence of the Jacobi matrix in Eq. (17).

In this context, it is natural to choose all of the $C_{jk}(0)$'s to be zero and to let them grow from the inhomogeneous $R_{ij}^{(2)}(t)$ terms.

F. Kurtz' limit theorem for the nonlinear fluctuation regime

When the covariances of the fluctuations have grown sufficiently large, the linear Fokker-Planck equation, Eq. (13), loses its validity. For jump processes satisfying Eq. (7), it has been shown that sample paths determined by the linear Fokker-Planck equation approximate sample paths for the underlying master equation to order $\Omega^{-1/2}$. However, when the fluctuations have grown too large for the linear approximation, another limit theorem has been proved from jump processes by Kurtz [5,6]. It is given by the nonlinear Fokker-Planck equation (by nonlinear we mean a nonlinear streaming term [4])

$$\frac{\partial}{\partial t}P_f(\mathbf{x},t)=-\frac{\partial}{\partial x_i}(K_i^{(1)}(\mathbf{x})P_f(\mathbf{x},t)) + \frac{1}{2}\frac{\partial^2}{\partial x_i \partial x_j}(K_{ij}^{(2)}(\mathbf{x})P_f(\mathbf{x},t)) \ , \tag{18}$$

in which the two W moments are functions of the probability space variables $\mathbf{x}$ and not of the deterministic solutions $\mathbf{x}(t)$. We have also denoted the probability distribution by $P_f(\mathbf{x},t)$ to signify that the large scale fluctuations are included in this description. Kurtz showed that sample paths determined by the nonlinear Fokker-Planck equation approximate sample paths for the underlying master equation to order $\ln(\Omega)/\Omega$. This is actually better than for the central limit theorem result, although it reduces to it when the fluctuations remain small, as, for example, during nonchaotic dynamics.

When the fluctuations are large enough, the macroscopic limit fails to emerge because

$$K_i^{(1)}(\mathbf{x}) \neq K_i^{(1)}(\mathbf{x}(t)) \tag{19}$$

and

$$\frac{d}{dt}\langle x_i \rangle_t = \langle K_i^{(1)}(\mathbf{x}) \rangle_t \neq K_i^{(1)}(\langle \mathbf{x} \rangle_t) \ , \tag{20}$$

where $\langle \ \rangle_t$ now denotes averaging with respect to $P_f(\mathbf{x},t)$. That is to say, there are no longer autonomous equations solely in terms of $\langle \mathbf{x} \rangle_t$ describing the macroscopic dynamics. Nevertheless, while $K_i^{(1)}(\mathbf{x}(t))$ no longer plays a role, its functional form still does through the presence of $K_i^{(1)}(\mathbf{x})$ in Eq. (18). Thus, the precursor to the classical dynamics, had it emerged, plays a dominant role in the evolution of the fluctuations, along with $K_{ij}^{(2)}(\mathbf{x})$.

Generally, numerical integration of this description is required because analytic solutions to Eq. (18) do not exist. Elsewhere [1] we have shown that it is far more tractable and efficient numerically to simulate a nonlinear Langevin equation that is equivalent to the Fokker-Planck equation, Eq. (18). This equation often takes the simple form [3]

$$\frac{d}{dt}\mathbf{x}=K_i^{(1)}(\mathbf{x})+(\text{noise terms}) \ . \tag{21}$$

The form of the noise terms is uniquely determined by $K_{ij}^{(1)}(\mathbf{x})$ and $K_{ij}^{(2)}(\mathbf{x})$. While this may look like we have simply added noise terms to the deterministic equations, it is much more subtle than that. It is only an approximation to the underlying master equation, and the master equation, or an equivalent mesoscopic description, is required in order to deduce the contribution to the noise terms made by $K_{ij}^{(2)}(\mathbf{x})$.

III. CHAOS AND THE QUANTUM-CLASSICAL CORRESPONDENCE LIMIT

A. Wigner-Liouville correspondence

The analysis of quantum-classical correspondence follows lines of reasoning [3] remarkably parallel to those just reviewed for intrinsic fluctuations in macroscopic dissipative systems. We begin by examining the traditional Wigner-Liouville correspondence, originally put forth by Wigner [7]. The Wigner distribution, defined in terms of the wave function, Ψ, by

$$W(x_1,\ldots,x_n,p_1,\ldots,p_n)=\left[\frac{1}{\hbar\pi}\right]^n \int \cdots \int dy_1 \cdots dy_n \Psi^*(x_1+y_1,\ldots,x_n+y_n)\Psi(x_1-y_1,\ldots,x_n-y_n) \times \exp\left[2\frac{i}{\hbar}(p_1y_1+\cdots+p_ny_n)\right] \tag{22}$$

is not a positive definite distribution in the phase-space variables, **x** and **p**, but its partial integral reductions:

$$\int \cdots \int dp_1 \cdots dp_n W \text{ and } \int \cdots \int dx_1 \cdots dx_n W$$

are, respectively, the correct probability distributions for the coordinates, **x**, and the momenta, **p**.

Consider a Hamiltonian system with Hamiltonian

$$H=\sum_{k=1}^{n}\frac{p_k^2}{2m_k}+V(x_1,\ldots,x_n)\ . \tag{23}$$

Wigner showed [7] that the time evolution of W is given by

$$\begin{aligned}\frac{\partial}{\partial t}W=&\sum_{k=1}^{n}\left[-\frac{p_k}{m_k}\frac{\partial W}{\partial x_k}+\left[\frac{\partial V}{\partial x_k}\right]\frac{\partial W}{\partial p_k}\right]\\&+\sum_{\lambda_1+\cdots+\lambda_n \text{ is odd}}\left[\frac{\partial\lambda_1+\cdots+\lambda_n V}{\partial x_1^{\lambda_1}\cdots\partial x_n^{\lambda_n}}\right]\\&\times\frac{\left[\frac{\hbar}{2i}\right]^{\lambda_1+\cdots+\lambda_n-1}}{\lambda_1!\cdots\lambda_n!}\\&\times\frac{\partial\lambda_1+\cdots+\lambda_n W}{\partial p_1^{\lambda_1}\cdots\partial p_n^{\lambda_n}}\ .\end{aligned} \tag{24}$$

In the limit $\hbar\to 0$ we obtain Liouville's equation

$$\frac{\partial}{\partial t}W_0=\sum_{k=1}^{n}\left[-\frac{p_k}{m_k}\frac{\partial W_0}{\partial x_k}+\left[\frac{\partial V}{\partial x_k}\right]\frac{\partial W_0}{\partial p_k}\right]\ . \tag{25}$$

Since this equation is first order in each of its derivatives, it can have Dirac delta function solutions [cf. Eq. (10)] that follow classical trajectories given by

$$\frac{d}{dt}x_k=\frac{p_k}{m_k}\ , \tag{26}$$

$$\frac{d}{dt}p_k=-\frac{\partial V(x_1,\ldots,x_n)}{\partial x_k}\ . \tag{27}$$

It is in this sense that we see classical physics *emerge* from the underlying quantum description in the $\hbar\to 0$ limit.

B. Central limit theorem treatment of the quantum fluctuations

In parallel with the treatment for fluctuations given in Sec. II D, we introduce the scaling [3]

$$x_i=x_i(t)+\hbar^{1/2}\mu_i\ , \tag{28}$$

$$p_i=p_i(t)+\hbar^{1/2}\nu_i\ , \tag{29}$$

in which $\hbar$ now plays the role of the smallness parameter previously played by $\Omega^{-1/2}$. The fluctuations distribution, $\Phi(\mu,\nu,t)$, satisfies the time evolution equation

$$\frac{\partial}{\partial t}\Phi=-\frac{\nu_k}{m_k}\frac{\partial\Phi}{\partial\mu_k}+\left[\frac{\partial^2 V}{\partial x_j\partial x_k}\right]\mu_j\frac{\partial\Phi}{\partial\nu_k}+O(\hbar^{1/2})\ , \tag{30}$$

which is the analogous of Eq. (13). The initial distribution must satisfy Heinsenberg's principle, i.e.,

$$\Phi(\mu,\nu,0)=\prod_{j=1}^{n}\frac{1}{4\pi}\exp\left[-\frac{\mu_j^2}{2\sigma^2}-2\sigma^2\nu_j^2\right] \tag{31}$$

with

$$\langle(\Delta\mu_i)^2\rangle^{1/2}\langle(\Delta\nu_i)^2\rangle^{1/2}=\sigma\frac{1}{2\sigma}=\frac{1}{2}\ . \tag{32}$$

C. Symplectic structure of Hamiltonian dynamics

Hamiltonian dynamics is symplectic, which implies the change of variables:

$$z_i=\begin{cases}x_i & \text{for } i=1,2,\ldots,n \qquad (33)\\ p_{i-n} & \text{for } i=n+1,n+2,\ldots,2n\ . \qquad (34)\end{cases}$$

Let the matrix I be defined by

$$I=\begin{bmatrix}0 & E\\ -E & 0\end{bmatrix}\ , \tag{35}$$

in which 0 is the $n\times n$ zero matrix and E is the $n\times n$ identity matrix. Hamilton's equations now can be rendered as

$$\frac{d}{dt}z_i=I_{ij}\frac{\partial H}{\partial z_j}\ . \tag{36}$$

The Hamiltonian Jacobi matrix is

$$J_{ij}=I_{ik}\frac{\partial^2 H}{\partial z_j\partial z_k}\ , \tag{37}$$

in which the sum over k is implicit, and the scaling becomes

$$z_i=z_i(t)+\hbar^{1/2}\eta_i \tag{38}$$

where

$$\eta_i=\begin{cases}\mu_i & \text{for } i=1,2,\ldots,n \qquad (39)\\ \nu_{i-n} & \text{for } i=n+1,n+2,\ldots,2n \qquad (40)\end{cases}$$

follows from Eqs. (33) and (34). The quantum fluctuations equation, Eq. (30), now takes the simple form

$$\frac{\partial}{\partial t}\Phi(\eta,t)=-J_{ij}(t)\eta_i\frac{\partial\Phi(\eta,t)}{\partial\eta_j}\ , \tag{41}$$

in which the Jacobi matrix, **J**, is a function of t through its dependence upon the classical solutions to Eqs. (26) and (27). This implies that the covariance matrix time evolution equation is

$$\frac{d}{dt}C_{ij}=J_{ik}C_{kj}+C_{ik}J_{jk}\ , \tag{42}$$

where

$$C_{ij}=\langle\eta_i\eta_j\rangle \tag{43}$$

and has initial value [cf. Eq. (17)]

$$\mathbf{C}(0)=\begin{bmatrix}\sigma^2 E & 0\\ 0 & \frac{1}{\sigma^2}E\end{bmatrix}, \tag{44}$$

which contains $n\times n$ dimensional blocks.

From the results presented in Sec. II, we should expect the initial exponential rate of growth of the covariances to be closely related to twice the largest classical Liapunov exponent determined for the corresponding classical flow.

This linear description of the fluctuations becomes invalid once the fluctuations have grown so large that the threshold for nonlinearities has been crossed. In that eventually, instead of using an analogue to Kurtz' theorem for nonlinear fluctuations, we simply solve the Schrödinger equation directly. In Sec. II this would have amounted to solving the Master equation directly rather than the approximate Langevin equation, Eq. (21)

D. Husimi-O'Connell-Wigner distributions

W is not positive definite. The Husimi-O'Connell-Wigner distribution function is positive definite [8,9]. The Gaussian smoothing of the Wigner distribution in one degree of freedom takes the form

$$W_S(x,p,\sigma)=\left[\frac{1}{\hbar\pi}\right]\int\int dx'dp'W(x',p')\times\exp\left[-\frac{(x'-x)^2}{2\sigma^2}-\frac{(p'-p)^2}{2\beta^2}\right]. \tag{45}$$

Heinsenberg's principle requires $\beta\geq\hbar/2\sigma$. O'Connell and Wigner [9] have shown that the time evolution for the smoothed Wigner distribution, to lowest order in σ and β, is

$$\frac{\partial}{\partial t}W_S=-\frac{1}{m}\left[p+\beta^2\frac{\partial}{\partial p}\right]\frac{\partial}{\partial x}W_S+\left[\frac{\partial V}{\partial x}+2\sigma^2\left[\frac{\partial^2 V}{\partial x^2}\right]\frac{\partial}{\partial x}\right]\frac{\partial}{\partial p}W_S\,. \tag{46}$$

O'Connell and Wigner explicitly used $\beta=\hbar/2\sigma$ in the first term on the right-hand side and omitted the σ^2 contribution in the second term. This led them to the observation [9] "the time dependence of W_S, in contrast to that of W, is not given by the classical expression [Eq. (25) of Sec. III A] but contains a correction term of order $\hbar^2$. But this is not a quantum effect:. . . ." As we also see, it is really just a β^2 effect corresponding to the momentum variance, but in addition there is also a σ^2 effect from the coordinate variance, as in Eq. (46).

By applying O'Connell and Wigner's analysis for the time evolution of W_S, to the Liouvillean evolution of an initially Gaussian phase space ensemble, we find that there is perfect correspondence to orders β^2 and σ^2. For any initial distribution, one can use the Green function for Liouville's equation to propagate the initial distribution into the one at time t. The Green function for this is just the Dirac δ function solution for a classical trajectory emanating from an arbitrary source point in phase space. The convolution of this with the initial distribution is the answer to the problem. However, if instead, the description is given in terms of an autonomous equation for the smoothed Liouville distribution, smoothed with an initial, Gaussian distribution, then one gets the O'Connell-Wigner equation, Eq. (46), to orders β^2 and σ^2. The physical interpretation in both the quantum and the classical cases is that the Gaussian smoothing of W, or the equivalent Gaussian smoothing of the Liouville distribution, reflect an unavoidable uncertainty in the initial conditions. In short, absolute mathematical precision is physically forbidden. The connection between the Husimi-O'Connell-Wigner distribution function and the Liouville distribution for an ensemble establishes the proper context for quantum-classical correspondence.

In Sec. II F, we recalled that it is easier to numerically implement a stochastic Langevin equation than it is to integrate a partial differential equation, i.e., Kurtz' nonlinear Fokker-Planck equation. In the quantum case we find it easier to implement the Schrödinger time evolution of an initially Gaussian wave packet than to numerically integrate the O'Connell-Wigner equation. The results from this approach are given in Sec. IV.

In Sec. II, we found that an approximate treatment of the nonlinear fluctuation regime is given by the nonlinear Langevin equation, Eq. (21). While no comparable parallel equation is presented in this section for the quantum-classical correspondence, because we use Schrödinger's equation directly, it is nevertheless of interest to ask what its form might take. Two possibilities, requiring deeper investigation, are (1) The van Vleck construction as developed by Heller and Tomsovic [16], and (2) a stochastic Schrödinger equation construction developed by Carmichael [17] (this construction is similar to earlier work, by Faid and Fox [18], on a stochastic quantum theory for spectral line shapes).

IV. THE PERIODICALLY KICKED PENDULUM

A model system that has been extensively studied both quantum mechanically and classically is the periodically kicked pendulum. It has Hamiltonian [2]

$$H=\frac{P_\theta^2}{2mL^2}-\delta_p\left[\frac{t}{T}\right]mL^2\omega_0^2\cos\theta\,, \tag{47}$$

in which the periodic Dirac δ function, δ_p, appears

$$\delta_p\left[\frac{t}{T}\right]=\sum_{j=-\infty}^{\infty}\delta\left[j-\frac{t}{T}\right]. \tag{48}$$

T is the period of the kicks and the pendulum is a massless rod of length L with a point mass m attached at the end. We have introduced L and m in order to underscore our emphasis on the quantum-classical correspondence, in particular, the quantum behavior of a genuinely classical pendulum. In about half of the literature $\theta=0$ is the up position and in the other half, as here, $\theta=0$ is the down position.

A. The classical map

The classical map generated by integrating the dynamics implied by Hamiltonian H is called [10] the "standard map"

$$I_{n+1}=I_n-K\sin\theta_n \ , \tag{49}$$

$$\theta_{n+1}=(\theta_n+I_{n+1})\mathrm{mod}2\pi \ , \tag{50}$$

in which

$$\alpha=mL^2\omega_0^2T \ , \tag{51}$$

$$\beta=\frac{T}{mL^2} \ , \tag{52}$$

and

$$I=\beta P_\theta \ , \tag{53}$$

$$K=\alpha\beta \ . \tag{54}$$

This is the map from just before the kick n to just before kick $n+1$.

For all values of K below 1.0, some initial conditions lead to chaotic trajectories and others lead to nonchaotic trajectories. As K increases, the proportion of phase space associated with chaotic trajectories increases. The critical value, $K=0.9716\ldots$, is the value above which the chaotic regions are interconnected, i.e., global chaos containing islands of nonchaotic trajectories around stable elliptical centers. As K exceeds a value somewhat less than 5, the last stable elliptical center disappears and there is global chaos without islands.

B. The quantum map

The quantum map is expressed by expanding the wave function in terms of the free rotor eigenstate [2,10]

$$\psi(\theta,t)=\frac{1}{\sqrt{2\pi}}\sum_{n=-\infty}^{\infty}A_n(t)e^{in\theta} \ . \tag{55}$$

This produces the quantum map for the coefficients from just before kick n to just before kick $n+1$ [2,10,11].

$$A_r(n+1)=\sum_{n=-\infty}^{\infty}A_q(n)i^{r-q}J_{r-q}(\kappa)\exp\left[-\frac{ir^2\tau}{2}\right] \ , \tag{56}$$

in which κ and τ are defined by

$$\kappa=\frac{mL^2\omega_0^2T}{\hbar} \ , \tag{57}$$

$$\tau=\frac{\hbar T}{mL^2} \ . \tag{58}$$

We have studied the quantum map for initially Gaussian wave packets. The initial wave packet is given by [2]

$$A_n(0)=\left[\frac{\pi}{2\sigma^2}\right]^{-1/4}\exp(iba)\times\exp(-ina)\exp[-\sigma^2(b-n)^2] \ , \tag{59}$$

which agrees with the choice of 2's in Eq. (45). This wave packet has expectation values and variances given by

$$\langle\theta(0)\rangle\cong a \ , \tag{60}$$

$$\langle P_\theta(0)\rangle\cong\hbar b \ , \tag{61}$$

$$\langle\Delta\theta^2(0)\rangle\cong\sigma^2 \ , \tag{62}$$

$$\langle\Delta P_\theta^2(0)\rangle\cong\frac{\hbar^2}{4\sigma^2} \ . \tag{63}$$

We showed [2] that if the system is sufficiently subcritical and if both variances are sufficiently small then the wave packet propagates as a Gaussian wave packet for hundreds of kicks. An example [2] of this behavior is given for $\hbar=10^{-6}$, $\sigma=10^{-2}$, $\theta(0)=\pi/2$, $P_\theta(0)=1.0$, $\kappa=10^2$, and $\tau=10^{-6}$. Since $P_\theta(0)$ is 10^6 times bigger than $\hbar$, we consider this to be an example of a macroscopic classical pendulum. It is very subcritical since $K=10^{-4}$. For this case, it is impossible to distinguish a phase-space plot of the classical map from a plot of the angle and angular-momentum expectation values for the quantum map, for hundreds of kicks. Since the wave packet approximately evolves as a Gaussian for all of these kicks, the angle variance grows algebraically so that after n kicks [2]

$$\sigma^2(n)=\sigma^2\left[1+\frac{n^2\tau^2}{4\sigma^4}\right] \ . \tag{64}$$

For the parameter values used above, it takes 200 kicks for the variance to double. This sort of growth of the variance is typical of what one expects very generally, in the absence of classical chaos. The chaotic situation is dramatically different, except for so-called "rationally resonant" cases [19,20].

C. Exponential growth of the variances

If we choose parameter values such that we are subcritical but have a classically chaotic trajectory, then we see exponential growth of the variances in the corresponding quantum treatment. An example of this is given for an initial condition which is very close to a hyperbolic separatrix [2]. The parameters are $\theta=\pi$ and $P_\theta=0.251320$ initially, and $\alpha=5\times10^{-3}$ and $\beta=50$ so that $K=0.25$. The largest Liapunov exponent is known to be $\lambda=0.046$. In order to compare the corresponding quantum treatment, we have used an initially Gaussian wave packet with $\hbar=10^{-5}$, $\sigma=0.01$, $\sigma_\theta=\sigma$, and $\sigma_P=\hbar/2\sigma_\theta$. A plot of the natural logarithm of the angular-momentum standard deviation (the square root of the variance) versus kick for the first 30 kicks is shown in Fig. 1.

Figure 1 illustrates several generic features. The first ten kicks exhibit an almost exponential growth from a kick 1 value of $e^{-7.6}$ up to the value at the tenth kick, $e^{-4.2}$. This is a multiplication by $e^{7.6-4.2}=10^{1.48}$, or nearly $1\frac{1}{2}$ orders of magnitude. Figure 2 shows the plot of the natural logarithm of the angle's standard deviation versus kick. Here we see a multiplication by $e^{4.31}=10^{1.87}$ for kicks 1–10. Again, the quality of the initial exponential stage is high, even though one may object that a mere factor of $10^{1.87}$ is not too impressive. A uniform angular

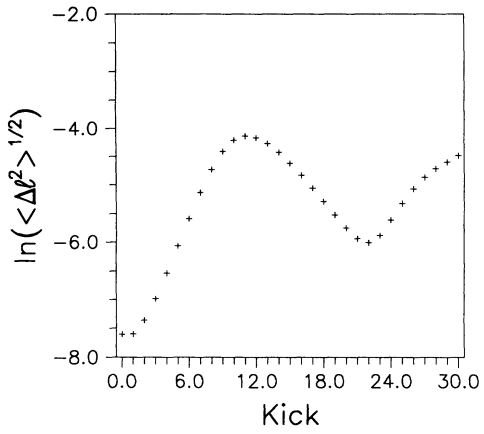

FIG. 1. A plot of the natural logarithm of the angular-momentum standard deviation versus kick for an initially Gaussian wave packet with $\hbar=10^{-5}$, $\sigma=0.01$, $\sigma_\theta=\sigma$, $\sigma_P=\hbar/2\sigma_\theta$, $\alpha=5\times10^{-3}$, and $\beta=50$. The initial wave packet is centered at $\theta=\pi$ and $P_\theta=0.251\,320$.

distribution has a standard deviation of 1.8. . . radians. Figure 2 shows a maximum at the tenth kick of $e^{0.71}=2.01$ rad. Thus, the angular standard deviation has effectively saturated by the tenth kick. Since the initial standard deviation was 10^{-2}, as is indicated for kick 0 in the figure, the overall increase by a factor of $10^{2.3}=200$ is all that could be expected. We return to this point below when we show results for a smaller initial standard deviation. This means σ_θ must be smaller and so must $\hbar$ so that $\hbar/2\sigma_\theta$ is smaller as well. All of this makes the numerical integration in the quantum case much more demanding.

Clearly, after ten kicks, say, the angular distribution has broadened out so much that it has saturated the available interval of width 2π. The expectation value of the angle for this wave packet becomes essentially π (the "up" position). As a function of time, this expectation value bears no resemblance to the classical map's sequence of angles, a chaotically random sequence of large-angle jumps. Thus, there is no longer any correspondence between the quantum wave-packet expectation value trajectory and the single classical trajectory. However, if instead we look at an initially Gaussian, classical ensemble with initial standard deviations σ_θ and σ_P then the classical map creates the time evolution of this classical ensemble. We find that the classical ensemble initially broadens, also exponentially, and eventually saturates the available domain. Averages over this ensemble show remarkable quantitative correspondence to the averages generated by the corresponding wave packet. Figures 3 and 4 show angular-momentum distributions at kicks 2, 4, 6, 8, and 10 for the quantum wave packet and for the classical ensemble, respectively. The reason for the saturation at kick 10 of the exponential stage of growth for the angular momentum is now evident. The angular-momentum distribution is bounded by KAM (Kol'mogorov-Arnol'd-Moser) curves which are reached by the distribution. The correspondence between the quantum wave packet and the classical ensemble in this regard is remarkable. Nevertheless, Figs. 3(e) and 4(e) show quantum inferences absent in the classical ensemble. There is some penetration of the KAM boundaries quantum mechanically but it is extraordinarily small for our parameter values [21].

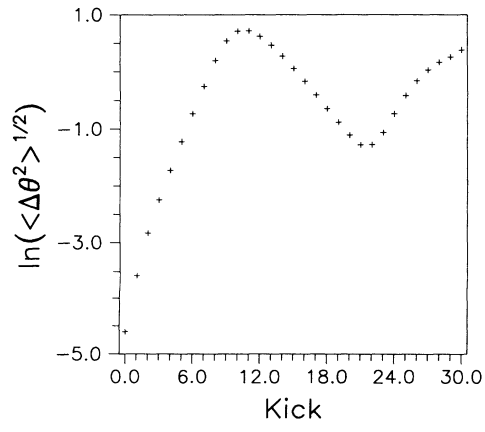

FIG. 2. A plot of the natural logarithm of the angle standard deviation versus kick for the same parameters used in Fig. 1.

In Figs. 5 and 6, respectively, we show the plots for the natural logarithms of the angular-momentum standard deviation and the angle standard deviation produced by the initially Gaussian, classical ensemble. The quantitative agreement with Figs. 1 and 2 is so good that they are visually indistinguishable for the first 29 kicks. Even the relative values for kick 0 and kick 1 are the same as in Figs. 1 and 2. From the classical perspective we can understand these features as follows. In the classical phase space there are one-dimensional, stable, and unstable manifolds. Initially, the unstable manifold is primarily in the direction of the angle expansion. Thus, the first kick primarily extends the distribution along the angle axis.

When there is not chaos in the classical trajectory, or in its nearby neighboring trajectories, then the quantum wave packet and the classical ensemble remain sharply peaked, nearly propagating as Gaussians, and distinction between trajectory and ensemble is negligible [2]. When chaotic trajectories densely populate the neighborhood of a particular trajectory, then both the quantum wave packet and the classical ensemble have first moment trajectories that bear no correspondence to this particular classical trajectory. Instead, the correspondence is between an initially Gaussian wave packet and an initially Gaussian classical ensemble.

It is much easier to study the exponential stage of growth for the classical ensemble than for the quantum wave packet. In Figs. 7 and 8 we show the growth of both the angular-momentum standard deviation and the angle standard deviation for $\sigma_\theta=10^{-5}$ and $\sigma_P=10^{-5}$. Quantum mechanically, this would require that $\hbar=10^{-10}$, which, for us, is numerically prohibitive. Nevertheless, all of our other results support the claim that the initial stage of exponential growth of the variances is the same for the quantum wave packet and for the classical ensemble. We see from the figure an exponential stage lasting 17 kicks and exhibiting a multiplication factor of 10^3 for the angular-momentum standard deviation,

and of $10^{3.7}$ for the angle standard deviation. Note that for the angle standard deviation there is a large increase with the first kick so that the overall multiplication factor from kick 0 to kick 17 is more than 10^5. Again, this is what is to be expected for $\sigma_\theta = 10^{-5}$ and a saturation value for the angle's standard deviation of order unity.

In Figs. 9 and 10 we show, respectively, the quantities in Figs. 1 and 5 for 500 kicks. In fact, the close correspondence between the Gaussian wave packet and the classical ensemble ceases after 29 kicks and they each develop their own characteristics. Thus, eventually there is even a breakdown of the correspondence between quantum wave packet and classical ensemble as a result of the difference in the origin of their fluctuations. For the classical ensemble, the fluctuations are exclusively a result of the distribution in initial conditions. For the quantum wave packet, there is an additional source: the incessant quantum perturbations in the dynamics of each and every kick. The differences seen in the figures have been subjected to scrutiny regarding numerical precision. We believe they are real and do not reflect numerical error propagation.

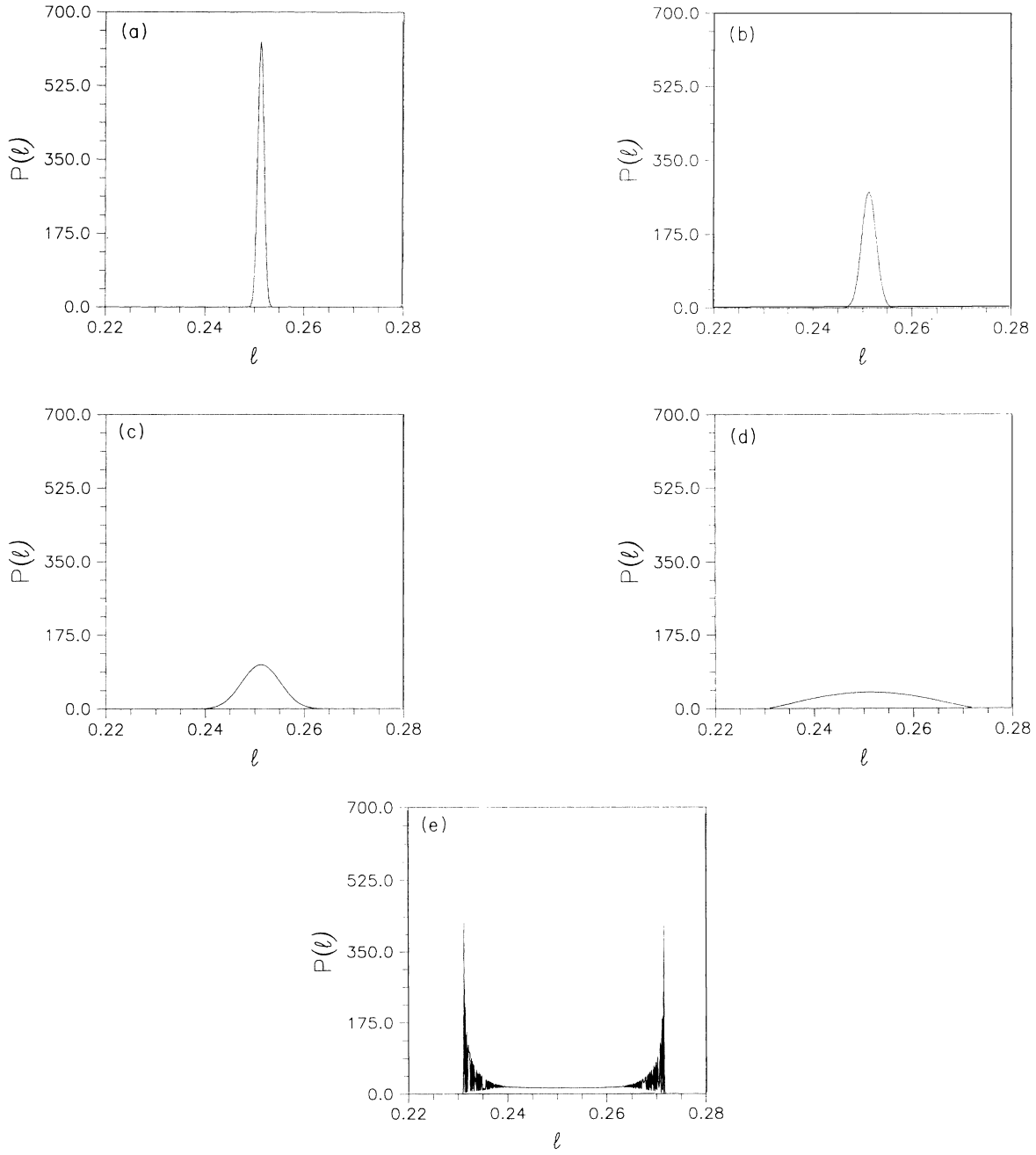

FIG. 3. The angular-momentum distribution for the parameters used in Fig. 1 is shown after kicks 2, 4, 6, 8, and 10, respectively, in plots (a), (b), (c), (d), and (e).

D. Transient expansion rate

How does the slope of the exponential growth stage of the standard deviation compare with the Liapunov exponent? As was stated above, the Liapunov exponent for the choice of parameters governing Figs. 1–6 is $\lambda=0.046$. However, the slope is 0.48 (as determined from kick 1 to kick 9, which is nearly straight in Fig. 1). This is an order of magnitude larger. The explanation involves the concept of a transient expansion rate.

For maps, the connection between the Jacobi matrix and the largest Liapunov exponent discussed in Sec. II, takes on a more computationally accessible form. Let the Jacobi matrix for the nth kick of the classical map given by Eqs. (49)–(54), $\mathbf{J}_n$, be defined by

$$\mathbf{J}_n=\begin{bmatrix}1 & -\alpha\cos\theta_n \\ \beta & 1-\alpha\beta\cos\theta_n\end{bmatrix} . \tag{65}$$

The largest Liapunov exponent, λ, is defined by

$$\lambda=\lim_{n\to\infty}\frac{1}{n}\ln[\text{abs}(\text{trace }\mathbf{M}_n)] , \tag{66}$$

in which we see the natural logarithm of the absolute

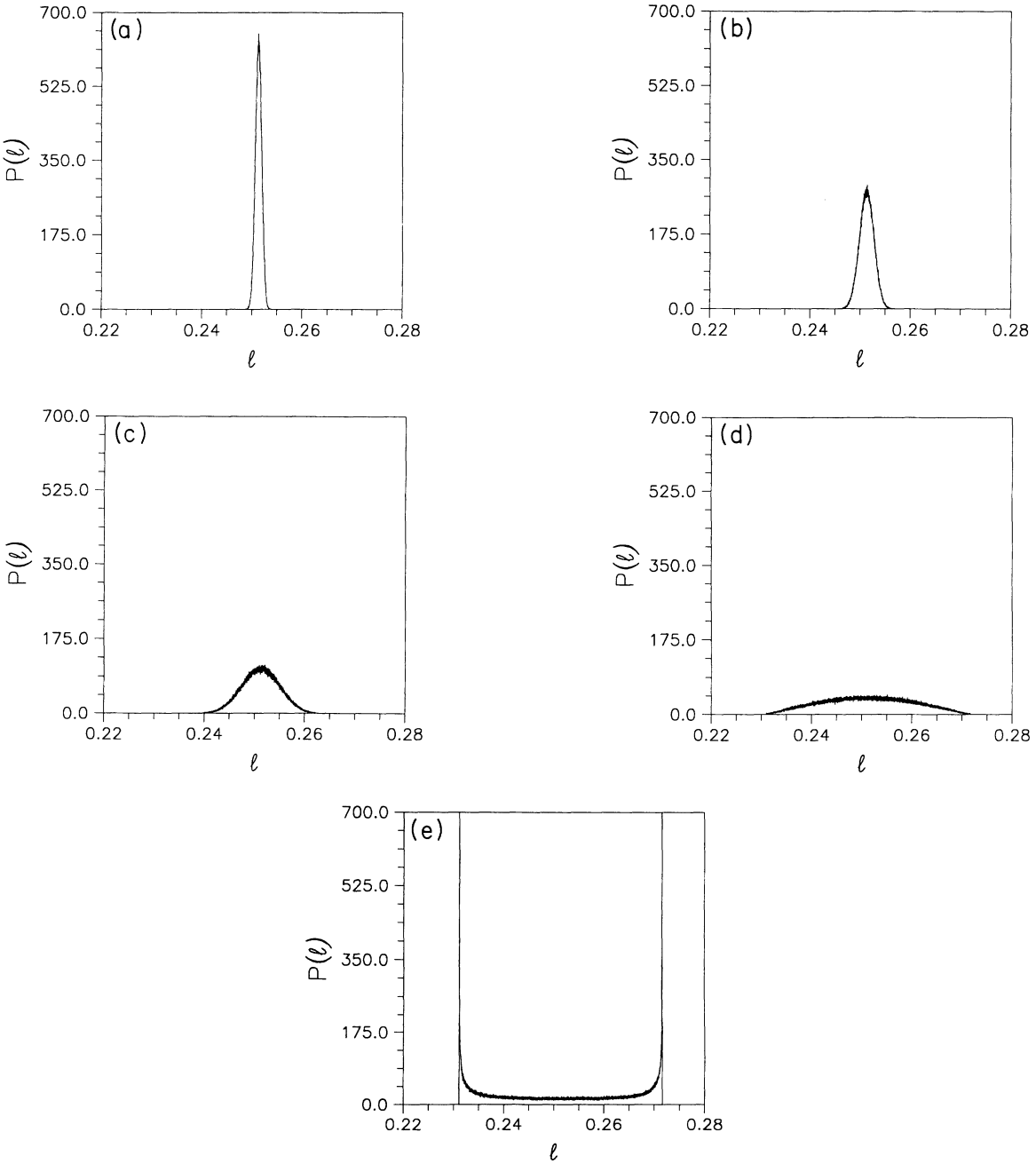

FIG. 4. These are the same plots as in Fig. 3 except that they are for the corresponding classical ensemble.

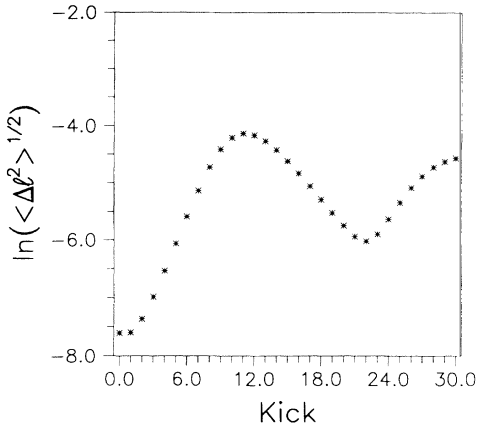

FIG. 5. A plot of the natural logarithm of the angular-momentum standard deviation versus kick for an initially Gaussian classical ensemble corresponding to the wave packet used in Fig. 1.

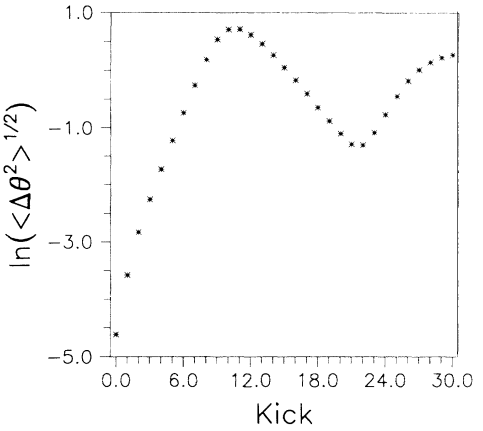

FIG. 6. A plot of the natural logarithm of the angle standard deviation versus kick for an initially Gaussian classical ensemble corresponding to the wave packet used in Fig. 2.

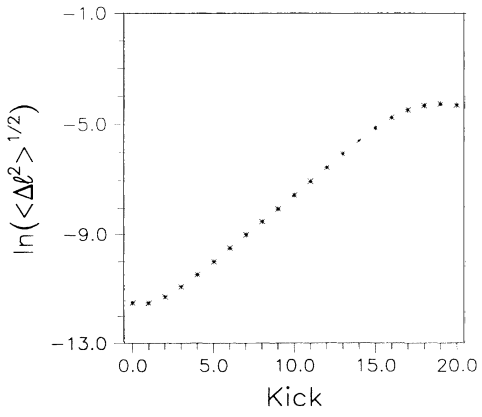

FIG. 7. A plot of the natural logarithm of the angular-momentum standard deviation versus kick for an initially Gaussian classical ensemble such as used in Fig. 5 but with $\sigma_\theta = 10^{-5}$ and $\sigma_P = 10^{-5}$.

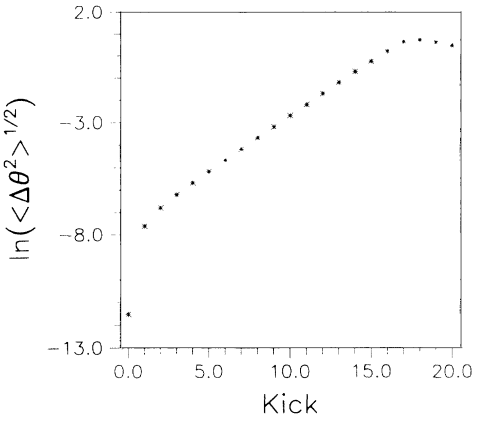

FIG. 8. A plot of the natural logarithm of the angle standard deviation versus kick for an initially Gaussian classical ensemble such as used in Fig. 6 but with $\sigma_\theta = 10^{-5}$ and $\sigma_P = 10^{-5}$.

value of the trace of $\mathbf{M}_n$, which is the nth order iterate of the time evolving Jacobi matrix

$$\mathbf{M}_n = \mathbf{J}_n \mathbf{J}_{n-1} \cdots \mathbf{J}_2 \mathbf{J}_1 \ . \tag{67}$$

Only the largest eigenvalue of $\mathbf{M}_n$ contributes in the limit. The value $\lambda = 0.046$ is the large n limit of the right-hand side of (66) for a single classical trajectory emanating from the initial conditions $\theta = \pi$ and $P_\theta = 0.251320$.

The transient expansion rate is generated somewhat differently. First of all, we evaluate the largest eigenvalue of $\mathbf{M}_n$ for each kick n. Then we do it again for another initial condition drawn from the classical Gaussian ensemble with $\sigma = 0.01$, $\sigma_\theta = \sigma$, $\sigma_P = \hbar/2\sigma_\theta$. These values are averaged together to produce the transient expansion rate, λ_n, given by

$$\lambda_n = \left\langle \frac{1}{n} \ln(\text{largest eigenvalue of } \mathbf{M}_n) \right\rangle \tag{68}$$

in which $\langle\ \rangle$ denotes the ensemble average. We discover that λ_9, for example, is 0.48, in very good agreement with the slope in Fig. 1, but that λ_{50} is 0.046, in excellent agreement with the asymptotic value for the largest

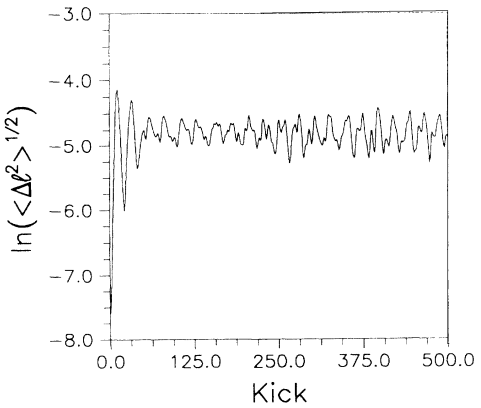

FIG. 9. This is the same as Fig. 1 but for 500 kicks.

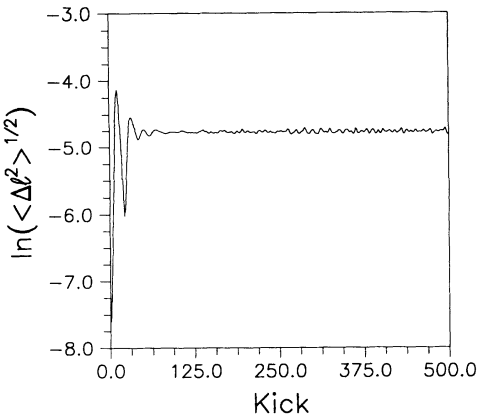

FIG. 10. This is the same as Fig. 5 but for 500 kicks.

Liapunov exponent. By the 50th kick the ensemble has spread out and is sampling the entire attractor, but up to the ninth kick it is actively expanding locally and does not represent a global sampling. Instead, it reflects the local rate of expansion near the initial conditions, averaged over an initially very sharp Gaussian ensemble. Figure 11 depicts the transient expansion rate. In the early stages, i.e., for small n, the larger expansion rates associated with the exponential growth stage, are clearly visible. Asymptotically, the expansion rate approaches the largest positive Liapunov exponent value.

In Figs. 12, 13, and 14, we show, respectively: the natural logarithm of the angular-momentum standard deviation versus kick, a blowup of the initial segment, and the transient expansion rate for a supercritical quantum case with $K=2$. Notice especially in Fig. 12 that there are two stages for the growth rate, the first one which is an exponential growth stage, and a second one, the nature of which is elucidated below. In Fig. 13, we show an exponential stage of three kicks for $\hbar=10^{-5}$ in plot a, and an exponential stage of five kicks for $\hbar=10^{-6}$ in plot b. This illustrates how decreasing the initial variances [cf. Eq. (63)] increases the extent of the exponential stage of growth. The corresponding classical ensemble behaves in

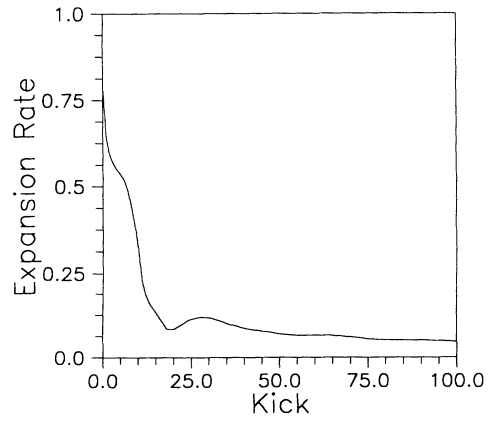

FIG. 11. A plot of the transient expansion rate versus kick for the parameters used in Fig. 1.

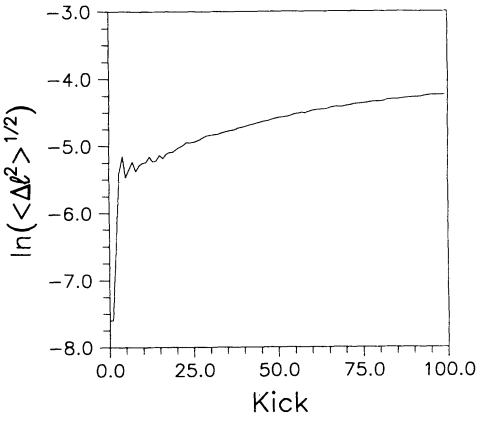

FIG. 12. A plot of the natural logarithm of the angular momentum standard deviation versus kick for an initially Gaussian wave packet with $\hbar=10^{-5}$, $\sigma=0.01$, $\sigma_\theta=\sigma$, $\sigma_P=\hbar/2\sigma_\theta$, $\alpha=5\times10^{-3}$, and $\beta=200$. The initial wave packet is centered at $\theta=\pi$ and $P_\theta=0.251\,320$.

the same way, almost exactly the same for nearly a hundred kicks.

E. The diffusive growth stage

That "initially exponential growth of the quantum standard deviations" is the generic signature of classical

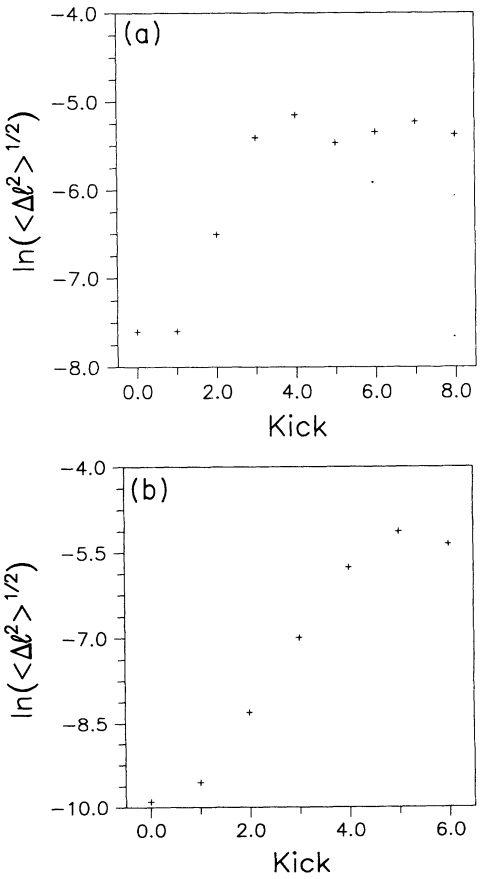

FIG. 13. A blowup of the initial segment of Fig. 12 for $\hbar=10^{-5}$ in plot (a), and for $\hbar=10^{-6}$ in plot (b).

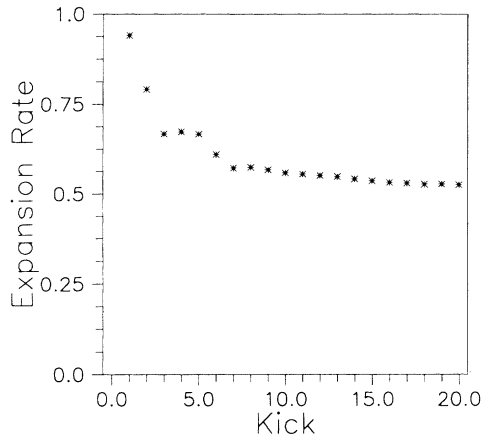

FIG. 14. A plot of the transient expansion rate versus kick for the parameters used in Figs. 12 and 13.

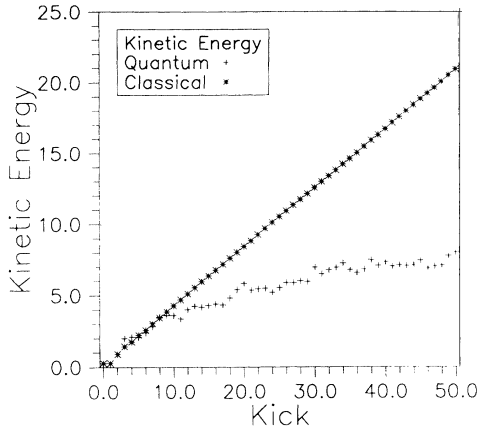

FIG. 16. A plot of the kinetic energy versus kick for a Gaussian wave packet centered initially at zero angle and zero angular momentum with standard deviations $\sigma=0.01$, $\sigma_\theta=\sigma$, and $\sigma_P=\hbar/2\sigma_\theta$. All other parameters agree with those used in Fig. 15. The straight line is for a corresponding classical ensemble of 100 000 points.

chaos in a corresponding quantum analysis is not the characterization found in the extant literature. Rather, it is said, a diffusive growth stage is generic [10–12], except at rational resonances [19,20]. By diffusive is meant that the angular-momentum variance grows linearly with kick number. In the rationally resonant cases, for which $\tau=(M/N)4\pi$ in which M and N are integers, the variance grows quadratically with kick number. Both of these growth rates are simple power laws, like for the propagating Gaussian wave-packet rate, Eq. (64). None is as dramatic as the exponential growth rate. Instead of, for example, doubling the variance in 200 kicks, the variance may grow by 10^6 in ten kicks.

Figure 15 shows the kinetic energy versus kick for a quantum eigenstate, the ground state, which for small K values surrounds a stable elliptical center. This is the case exhibited in the literature as representative of the generic situation [10–12]. Since the ground state has a vanishing angular-momentum expectation value, we may view this plot as a plot of the growth of the angular-momentum variance. The other parameters used [10–12] are $\hbar=0.15(\sqrt{5}-1)/2$, $\alpha=10/2\pi$, and $\beta=2\pi$, so that $K=10$, an ultrasupercritical case. Note that $\hbar$ is much larger than what we have used. There is no hint of an exponential growth stage. In Fig. 16 we show the growth of the kinetic energy for a Gaussian wave packet initially centered at zero angle and at zero angular-momentum expectation values, just as for the ground state. This Gaussian wave packet has standard deviations given by $\sigma=0.01$, $\sigma_\theta=\sigma$, and $\sigma_P=\hbar/2\sigma_\theta$. The indefinitely long straight line shows the growth of the kinetic energy for a classical ensemble of 100 000 elements. The quantum curve agrees with the classical up to a break time of order 10 kicks, although the compressed time scale in Fig. 15 erroneously suggests a linear growth stage of perhaps 50 kicks.

Both the ground state and this Gaussian wave packet fail to exhibit an exponential growth stage. This is a

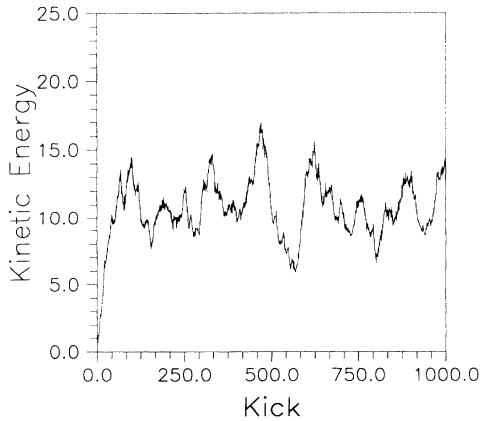

FIG. 15. A plot of the kinetic energy versus kick for the quantum free rotor ground state. The parameter values used here are $\hbar=0.15(\sqrt{5}-1)/2$, $\alpha=10/2\pi$, and $\beta=2\pi$, so that $K=10$.

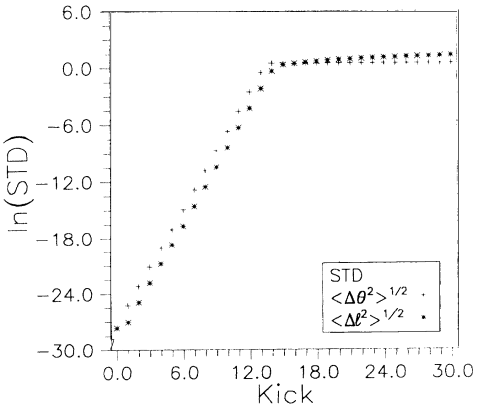

FIG. 17. A plot of the natural logarithms of the angle standard deviation and the angular momentum standard deviation versus kick for a classical ensemble corresponding to the wave packet used in Fig. 16 except that here we have $\sigma_\theta=10^{-12}$ and $\sigma_P=10^{-12}$.

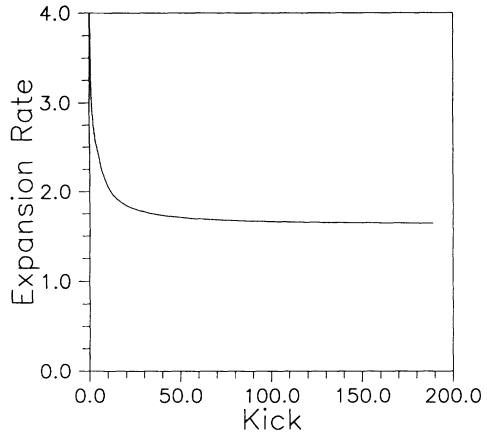

FIG. 18. A plot of the transient expansion rate for the case shown in Fig. 17.

consequence of the initially broad distribution in angle for the ground state, and the immediate growth to comparable size of this Gaussian wave packet for the effectively large standard deviation value $\sigma=0.01$, given the large value of $\hbar$. In Fig. 17, are shown results for a classical Gaussian ensemble based on $\sigma_\theta=10^{-12}$ and $\sigma_P=10^{-12}$ instead. Both the growth of the standard deviation for angle and for angular momentum are shown. For 14 kicks there is a dramatic exponential growth with a multiplication factor of 10^{12}. Note the sharp transition from exponential growth to diffusive growth for the angular-momentum standard deviation at kick 14. This transition is triggered by saturation of the angle distribution.

Figure 18 displays the transient expansion rate versus kick. At kick 14, the transient rate is 1.8, which is very close to the slope of the exponential stage in the figure. This is not too much larger than the asymptotic value, 1.609. Since this is an ultrasupercritical K value, Chirikov's formula is very accurately satisfied [13–15]. Because of the global chaos we have a nearly uniform expansion rate for the attractor. This is in contrast with the situation for subcritical K for which we found an order of magnitude difference between the transient and asymptotic values.

V. CONCLUDING REMARKS

Two well-established paradigms for the "quantum signature of classical chaos" are energy (or quasienergy) level spacing distributions [12], and eigenfunction scarring by unstable periodic classical orbits [16]. Much beautiful work has been done on each of these characterizations. In this paper, we present a third paradigm, the initially exponential growth of quantum variances for initially very sharply defined wave packets. This characterization is intimately connected to the problem of quantum-classical correspondence.

The present alternative paradigm is not in conflict with the well-known [10–12] diffusive growth of the kinetic energy for the quantum ground state, nor with the quadratic power-law growth for rationally resonant states [19,20]. Instead, these different behaviors result from initial conditions very different from those used by us to exhibit the exponential growth stage. Our initial conditions are designed to maximize quantum-classical correspondence. They reflect the physically unavoidable uncertainty in initial conditions, both quantum mechanically and classically. We find that corresponding to our initially very sharply peaked Gaussian wave packets are initially very sharply peaked classical Gaussian ensembles. Only for the classically nonchaotic domain do these two representations reduce to correspondence with a single classical trajectory, provided the Gaussian forms are sharp enough. For the chaotic domain, we find that during the initial exponential growth stage of the standard deviations, there is remarkably good correspondence between the wave packet and the ensemble, but eventually even this correspondence finally breaks down as a result of fundamental differences in the fluctuations.

We have also accounted quantitatively for the slope of the exponential growth stage. It is intimately tied to the time evolving Jacobi matrix for the classical ensemble, averaged over the ensemble. The transient expansion rate was introduced to illustrate and formalize this connection. Asymptotically, the transient rate becomes the largest Liapunov exponent.

This work elucidates how the classical concepts of phase space, exponential sensitivity to initial conditions, and Liapunov exponents may be incorporated in a quantum description. The key ideas are the central role of the Jacobi matrix and the natural correspondence between Husimi-O'Connell-Wigner distributions and Gaussian Liouville distributions.

ACKNOWLEDGMENTS

This work was supported by National Science Foundation Grant No. 92-03878. We thank Hal Gersch for bringing Ref. [9] to our attention.

[1] R. F. Fox and J. E. Keizer, Phys. Rev. Lett. **64**, 249 (1990); R. F. Fox, Phys. Rev. A **42**, 1946 (1990); R. F. Fox, *ibid.* **44**, 6193 (1991); C. Bracikowski, R. F. Fox, and R. Roy, *ibid.* **45**, 403 (1992); J. Keizer, R. F. Fox, and J. Wagner, Phys. Lett. A **175**, 17 (1993); R. F. Fox and T. C. Elston, Chaos **3**, 313 (1993); T. C. Elston and R. F. Fox, *ibid.* **4**, 1 (1994).

[2] R. F. Fox and B. L. Lan, Phys. Rev. A **41**, 2952 (1990); B. L. Lan and R. F. Fox, *ibid.* **43**, 646 (1991).

[3] R. F. Fox, Phys. Rev. A **41**, 2969 (1990); R. F. Fox and J. Keizer, *ibid.* **43**, 1709 (1991).

[4] N. G. van Kampen, *Stochastic Processes in Physics and Chemistry* (North-Holland, Amsterdam, 1981).

[5] T. G. Kurtz, Math. Prog. Stud. **5**, 67 (1976).

[6] T. G. Kurtz, Stoch. Proc. Appl. **6**, 223 (1978).

[7] E. P. Wigner, Phys. Rev. **40**, 749 (1932).

[8] K. Husimi, Proc. Phys. Math. Soc. Jpn. **22**, 264 (1940).
[9] R. F. O'Connell and E. P. Wigner, Phys. Lett. **85A**, 121 (1981).
[10] G. Casati, B. V. Chirikov, F. M. Izrailev, and J. Ford, in *Stochastic Behavior in Classical and Quantum Hamiltonian Systems,* Lecture Notes in Physics Vol. 93, edited by G. Casati and J. Ford (Springer-Verlag, New York, 1979), p. 334.
[11] T. Dittrich and R. Graham, in *Instabilities and Nonequilibrium Structures II,* edited by E. Tirapegui and D. Villarroel (Kluwer Academic, Dordrecht, 1989), p. 145; Ann. Phys. **200**, 363 (1990).
[12] F. Haake, *Quantum Signatures of Chaos* (Springer-Verlag, Berlin, 1991), Chap. 8.
[13] B. V. Chirikov, F. M. Izrailev, and D. L. Shepelyansky, Sov. Sci. Rev. C **2**, 209 (1981).
[14] F. M. Izrailev, Phys. Rep. **196**, 299 (1990).
[15] B. L. Lan (unpublished).
[16] E. Heller and S. Tomsovic, Physics Today **46**, 38 (1993), and references therein.
[17] H. J. Carmichael, *An Open Systems Approach to Quantum Optics* (Springer-Verlag, New York, 1993).
[18] K. Faid and R. F. Fox, Phys. A **34**, 4286 (1986).
[19] G. Casati, J. Ford, I. Guarneri, and F. Vavaldi, Phys. Rev. A **34**, 1413 (1986).
[20] F. M. Izrailev and D. L. Shepelyansky, Teor. Mat. Fiz. **43**, 417 (1980).
[21] G. Radons, T. Geisel, and J. Rubner, Adv. Chem. Phys. **73**, 891 (1989).